ARTICLE

Magnetic Nano-Amorphous-Iron-Oxide-Based Drug Delivery System with Dual Therapeutic Mechanisms

Shan Lei[a], Li-an Wang[a], Fu-xing Lin[b*], Kun Zeng[a], Mo-zhen Wang[a*], Xue-wu Ge[a]

a. CAS Key Laboratory of Soft Matter Chemistry, Department of Polymer Science and Engineering, University of Science and Technology of China, Hefei 230026, China
b. College of Resources and Chemical Engineering, Fujian Engineering Research Center for Advanced Fluorine-containing Materials, Sanming University, Sanming 365004, China

(Dated: Received on June 28, 2019; Accepted on August 16, 2019)

Smart nanoparticles that respond to pathophysiological parameters, such as pH, GSH, and H_2O_2, have been developed with the huge and urgent demand for the high-efficient drug delivery systems (DDS) for cancer therapy. Herein, cubic poly(ethylene glycol) (PEG)-modified mesoporous amorphous iron oxide (AFe) nanoparticles (AFe-PEG) have been successfully prepared as pH-stimulated drug carriers, which can combine doxorubicin (DOX) with a high loading capacity of 948 mg/g, forming a novel multifunctional AFe-PEG/DOX nanoparticulate DDS. In an acidic microenvironment, the AFe-PEG/DOX nanoparticles will not only release DOX efficiently, but also release Fe ions to catalyze the transformation of H_2O_2 to ·OH, acting as fenton reagents. *In vitro* experimental results proved that the AFe-PEG/DOX nanoparticles can achieve combination of chemotherapeutic (CTT) and chemodynamic therapeutic (CDT) effects on Hela tumor cells. Furthermore, the intrinsic magnetism of AFe-PEG/DOX makes its cellular internalization efficiency be improved under an external magnetic field. Therefore, this work develops a new and promising magnetically targeted delivery and dual CTT/CDT therapeutic nano-medicine platform based on amorphous iron oxide.

Key words: Cubic amorphous iron oxide nanoparticles, pH-responsive, Chemotherapy, Chemodynamic therapy, Magnetically targeted delivery

I. INTRODUCTION

Chemotherapy is one of the most commonly used pathways for cancer treatment, although it is controversial for a long time due to the systemically delivery and unpleasant side effects [1]. Nanocarrier-based drug delivery system (DDS) offers new opportunities to improve the biosafety, bioactivity, and prolonged bioavailability of the small molecular drugs [2–4]. However, low drug loading/release efficacy will restrict the anticancer efficiency of nano DDS [5–8]. Extensive efforts have been made to develop diverse stimuli-responsive drug carriers in order to explore satisfactory nano DDS [9]. A variety of external signals, such as light [10], ultrasound [11], and magnetic field [12], as well as physiological internal signals, such as pH [13], GSH [14, 15], H_2O_2 [16], enzyme [17], and ATP [3], have been utilized to regulate the drug loading/release of DDS. Among these signals, pH is the most frequently used one due to the distinctive acidic microenvironment in tumor cells [5, 13, 18–21]. Typically, tumor tissues have a lower extracellular pH value (≈6.8) than normal tissues, and a much lower pH (<5.4) in the endosomes and lysosomes. Therefore, pH-responsive nanocarriers, such as $CaCO_3$-based nanoparticles [22], hollow mesoporous Prussian blue (PB) [7, 8], Fe-based nanoparticles [6], and pH-cleavable linkers [19], have been widely used to construct the intracellular DDSs that undergo an endocytosis pathway, thereby achieving the controlled release of anticancer drugs in tumor cells.

Recently, the function of DDSs has been more than drug delivery. DDSs with various anticancer mechanisms, such as photothermal therapy [23], photodynamic therapy [19], and chemodynamic therapy [24], have been widely reported to improve the overall efficacy. Fe-based DDSs are of particular interest since they can achieve the combination of chemotherapy and chemodynamic therapy. They can efficiently release both the loaded drug and Fe^{3+} or Fe^{2+} ions in acid tumor microenvironment. The latter further catalyzes the homolysis of H_2O_2 to produce ·OH, resulting in excessive ROS level to achieve chemodynamic therapeutic effect on cancer cells [25]. Furthermore, most Fe-based DDSs have an intrinsic magnetism so that they can be expected to achieve magnetically targeted drug delivery so as to enhance anticancer efficiency. However, the current pH-responsive Fe-based DDSs have not been well designed.

*Authors to whom correspondence should be addressed. E-mail: 20180105@fjsmu.edu.cn, pstwmz@ustc.edu.cn

 ©2020 Chinese Physical Society

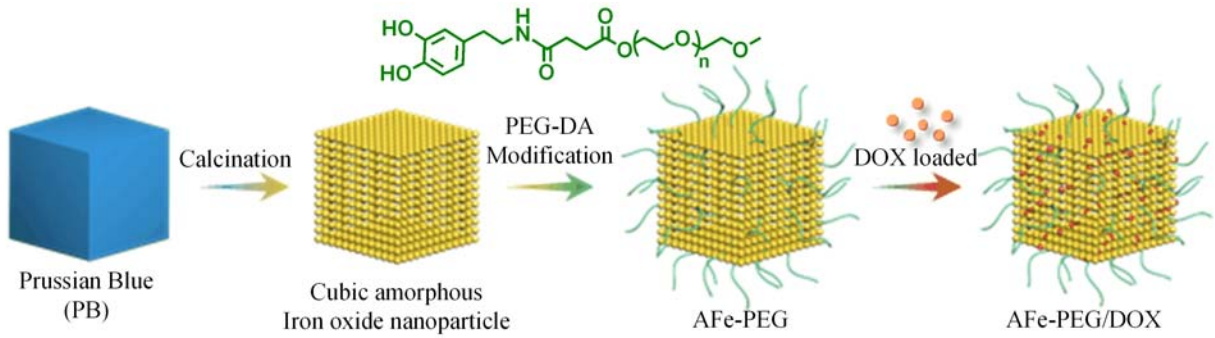

FIG. 1 Preparation process of AFe-PEG/DOX nanoparticle.

In this work, we have developed a versatile nanoplatform composed of polyethylene glycol (PEG) modified mesoporous amorphous iron oxides nanoparticles (AFe-PEG) with size of about 180 nm as the carrier of doxorubicin (DOX) (FIG. 1). The load capacity of AFe-PEG for DOX is as high as 948 mg/g, owing to its distinctive mesoporous structure and strong coordinative bonding between inherent Fe ions in AFe and chemical groups (*e.g.*, amino and carbonyl) of DOX at pH=7.4. With the decreasing of the external pH value (mildly acidic conditions), the metal-ligand coordination bonding will be broken, thus allowing DOX to release readily. At the same time, the Fe ions can also be released to react with H_2O_2 to produce ·OH. *In vitro* experimental results indicate that the AFe-PEG/DOX nanoparticles can achieve combination therapy effect to efficiently kill Hela cells. Furthermore, with applying an external magnetic field, the cellular internalization efficiency of the AFe-PEG/DOX nanoparticles will be increased, thereby achieving magnetically targeted drug delivery.

II. MATERIALS AND METHODS

A. Materials

Potassium ferricyanide, dimethyl sulfoxide (DMSO), tetrahydrafuran (THF), polyvinylpyrrolidone (PVP, K30), hydrochloric acid (36.0%−38.0%), phosphorus pentoxide, magnesium sulphate, pyridine, ethyl acetate, dichloromethane, hexane, diethyl ether, 4-dimethylaminopyridine (DMAP), NaH_2PO_4, Na_2HPO_4, sodium acetate trihydrate (NaAc), acetic acid (HAc) and chloroform were purchased from Sinopharm Chemical Reagent Co., Ltd. 1-Ethyl-3-(3-dimethyllaminopropyl) carbodiimide hydrochloride (EDC), doxorubicin hydrochloride (DOX·HCl), and 5,5-dimethyl-1-pyrroline N-oxide (DMPO) were purchased from Aladdin Reagent Company (Shanghai, China). Methoxypolyethylene glycols (mPEG, M_n=2000), dopamine hydrochloride, and succinic anhydride were purchased from Sigma-Aldrich. 3-(4,5-Dimethylthiazol-2-yl)-2,5-diphenyltetrazolium bromide (MTT), phosphate buffer saline (PBS) solution (0.01 mol/L, pH=7.4) and penicillin-streptomycin solution (1 mol/L) were purchased from Beyotime Institute of Biotechnology (Shanghai, China). Fetal bovine serum (FBS) and Dulbecco's modified Eagle's medium (DMEM) were purchased from GIBCO Co., Ltd. The complete DMEM was prepared by mixing DMEM, FBS and penicillin-streptomycin solution (1 mol/L) at volume ratio of 89:10:1. Hela cells were purchased from Cell Bank of Chinese Academy of Sciences (Shanghai, China). PBS solution (pH=6.5) was prepared by mixing NaH_2PO_4 (68.5 mL, 0.2 mol/L) and Na_2HPO_4 solution (31.5 mL, 0.2 mol/L). Acetate buffer solution (pH 5.4) was prepared by mixing NaAc (8.6 mL, 0.2 mol/L) and HAc solution (1.4 mL, 0.2 mol/L). PBS with a pH value of 7.4 was used in all cell culture experiments.

B. Preparation of Prussian blue (PB)

According to a modified method by Yamauchi group [26], PVP (3.0 g) and $K_3[Fe(CN)_6]$ (132 mg) were dissolved into 40 mL of HCl solution (0.01 mol/L) under ultrasonication. The solution was kept at 80 °C for 24 h. The product was precipitated and collected by centrifugation, then, washed with deionized water and ethanol three times, respectively, and finally dried in a vacuum oven at 60 °C for 12 h.

C. Preparation of cubic amorphous iron oxide (AFe) nanoparticles

According to the previous report [27], the above PB powder (100 mg) was heated to 400 °C in a resistance furnace at heating rate of 10 °C/min, kept for 4 h to let PB decompose into cubic AFe nanoparticles, and then cooled naturally.

D. Synthesis of dopamine-functionalized PEG (PEG-DA)

PEG-DA was synthesized using mPEG as the raw material through the following reactions:

DOI:10.1063/1674-0068/cjcp1906123 ©2020 Chinese Physical Society

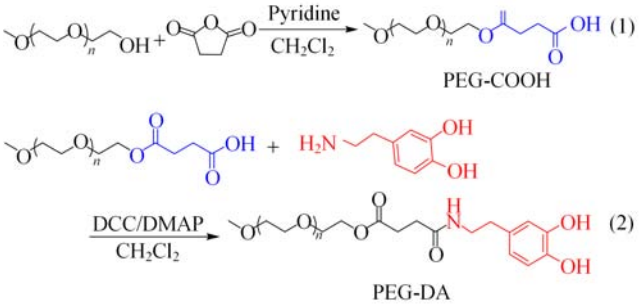

Briefly, mPEG (M_n=2000, 10.0 g, 5 mmol) and 2 equivalents of succinic anhydride (1.0 g, 10 mmol) (dried over P_2O_5 under high vacuum) were dissolved in 25 mL of anhydrous dichloromethane. Two equivalents of pyridine (0.8 mL, 10 mmol) was added as the catalyst. The system was refluxed for 3 d under nitrogen. The crude product was obtained by rotary evaporation of the solvent, and then dissolved in water. The aqueous solution of the crude product was washed with a mixture of ethyl acetate and hexane (V:V=1:1) for three times to eliminate the extra reactants. The product was extracted from the aqueous phase with $CHCl_3$. After the organic phase was dried with anhydrous $MgSO_4$ overnight, the solid product was obtained by the evaporation of $CHCl_3$ under reduced pressure, and recrystallized from diethyl ether to obtain the carboxyl-terminated PEG (PEG-COOH) (96% yield). The ^{1}H and ^{13}C NMR spectra of PEG-COOH (300 MHz, $CDCl_3$) are shown in FIG. S1 in supplementary materials. The detailed information is as follows: ^{1}H NMR (300 MHz, $CDCl_3$) δ(ppm): 4.30−4.22 (m, 2H), 3.66 (d, J=10.3 Hz, 179H), 3.56−3.52 (m, 2H), 3.38 (s, 3H), 2.69−2.59 (m, 4H). ^{13}C NMR (75 MHz, DMSO) δ(ppm): 169.00, 167.28, 67.06, 65.70, 65.70, 64.15, 23.93.

PEG-COOH (1.65 g, 0.78 mmol), EDC (0.18 g, 0.78 mmol) and DMAP (0.19 g, 1.55 mmol) were dissolved in 50 mL of CH_2Cl_2 under magnetic stirring. After the addition of 0.15 g of dopamine hydrochloride (0.78 mmol), the solution was continuously stirred for 24 h at room temperature under the protection of N_2. After that, the solution was washed with 1 mol/L HCl anhydrous solution three times. The aqueous phase was extracted by CH_2Cl_2. The organic phase was concentrated, and then precipitated in ether for three times to obtain PEG-DA with 80% yield. The ^{1}H and ^{13}C NMR spectra of PEG-DA (300 MHz, $CDCl_3$) are shown in FIG. S2 (supplementary materials). The detailed information is as follows: ^{1}H NMR (300 MHz, $CDCl_3$) δ(ppm): 6.79 (d, J=8.0 Hz, 1H), 6.71 (s, 1H), 6.55 (d, J=8.0 Hz, 1H), 4.22−4.15 (m, 2H), 3.64 (s, 187H), 3.56−3.52 (m, 2H), 3.44−3.34 (m, 5H), 2.67 (dd, J=11.3, 6.5 Hz, 4H), 2.43 (t, J=6.7 Hz, 2H). ^{13}C NMR (75 MHz, $CDCl_3$) δ/ppm: 172.84, 171.58, 144.57, 120.32, 115.90, 71.87, 70.50, 68.93, 63.66, 58.97, 40.81, 36.48, 34.72, 31.19, 29.70.

E. Preparation of AFe-PEG nanoparticles

AFe nanoparticles (50 mg) were dispersed into water (20 mL) by sonication for 10 min, followed by the addition of PEGCDA (100 mg). The mixture was stirred at room temperature for 12 h. After that, the products were collected by centrifugation and washed with deionized water three times, and then dried in a vacuum oven at 40 °C for 12 h.

F. Drug loading

AFe-PEG (10 mg) nanoparticles were dispersed in 6 mL of PBS (pH=7.4) containing 12 mg of DOX. The mixture was shaken in the dark at room temperature for 24 h to reach the equilibrium state. The DOX loaded AFe-PEG (AFe-PEG/DOX) nanoparticles were collected by centrifugation. The concentration of unloaded DOX in the supernatant (c_s) was measured according to the UV-Vis absorbance at 485 nm for DOX based on the working curve (FIG. S3 in supplementary materials). The loading capacity of DOX (Q_{DOX}) was calculated using the following Equation:

$$Q_{DOX} = \frac{(c_0 - c_s) \cdot V}{m_{AFe}} \quad (1)$$

Where, c_0 is the original concentration of DOX (2 mg/mL). V is the volume of the solution, *i.e.*, 6 mL. m_{AFe} is the total mass of AFe-PEG nanoparticles, *i.e.*, 10 mg.

G. Characterization

The morphologies of the prepared nanoparticles were observed by transmission electron microscopy (TEM, Hitachi H-7650, 100 kV). The UV-Vis absorption spectra were measured with Shimadzu UV-3600 PC spectrometer. The nitrogen adsorption-desorption isotherms were measured by Tristar II 3020 mol/L at 77.35 K after the samples were outgassed at 150 °C for 6 h. The specific surface area and pore size distribution were analyzed by BET and BJH methods, respectively. The total pore volume of the samples was calculated at p/p_0=0.97. X-ray diffraction (XRD) spectra were performed on a Rigaku SmartLab high resolution X-ray diffraction system using Cu Kα radiation at wavelength of 0.1541 nm. Fourier transform infrared (FTIR) spectra were recorded on a NICOLET 5700 FTIR Spectrometer using KBr pellets. Inductively coupled plasma optical emission spectrometry (ICP-OES) was measured on an Optima 7300 DV spectrometer to determine the content of Fe element. Magnetic hysteresis loop was measured on Vibrating Sample Magnetometer (VSM) at T=300 K. NMR spectra were performed on Bruker AVANCE NEO nuclear magnetic resonance spectrometer at 300 MHz for ^{1}H and 75 MHz for ^{13}C, respectively, using tetramethylsilane as the internal standard.

DOI:10.1063/1674-0068/cjcp1906123 ©2020 Chinese Physical Society

H. ESR spectroscopy

The electron spin resonance (ESR) technique was used to detect ·OH generated by the Fenton-reaction between AFe-PEG and H_2O_2, using DMPO as the radical trap. The sample was prepared by mixing 40 μL of aqueous solution of DMPO (100 mmol/L) and buffer solution (200 μL) containing 20 μL of H_2O_2 (5 mmol/L) and 1 μg of AFe-PEG in a dark eppendorf tube. ESR spectra were then measured at room temperature in perpendicular mode on a Bruker EMX-8/2.7 spectrometer at microwave frequency of 9072.732 MHz and microwave power of 0.998 mW. The magnetic field modulation frequency is 100.00 kHz with an amplitude of 1.00 G.

I. *In vitro* DOX release behavior of AFe-PEG/DOX

The DOX release behavior of AFe-PEG/DOX in different buffer solutions including acetate buffer solution (pH=5.4) and PBS (pH=6.5 and pH=7.4) was investigated. Typically, 10 mL of a certain buffer solution containing 5 mg of AFe-PEG/DOX nanoparticles was placed into the dialysis bag (MWCO=3500) and kept in the dark. Then, 0.5 mL of the dispersion was sampled out at a certain time interval. At the same time, 0.5 mL of fresh buffer solution was added in the original solution to keep constant volume. The absorbance intensity at 485 nm of the sampled solution was measured by UV-Vis spectroscopy in order to determine the accumulative released percentage of DOX after the nth sampling (q_n) according to the following Equation:

$$q_n = \frac{c_n V_0 + V\sum_{i}^{n} c_{i-1}}{mQ_{\mathrm{DOX}}} \times 100\% \qquad (2)$$
$$c_0 = 0,$$
$$i = 1, 2, \ldots, n$$

where, c_n is the concentration of DOX with a unit of mg/mL at the nth sampling. V_0 is the initial volume of the solution, *i.e.*, 10 mL. V is the volume of the sampled solution, *i.e.*, 0.5 mL. m is the mass of the added AFe-PEG/DOX nanoparticles, *i.e.* 5 mg.

J. *In vitro* combined chemodynamic and chemotherapy assay

Hela cells were cultured in a 96-well plate with the complete DMEM medium at 37 °C with 5% CO_2 humidified atmosphere for 24 h. After that, the culture medium was replaced by four kinds of media, *i.e.*, PBS, PBS containing a certain concentration of AFe-PEG, DOX, and AFe-PEG/DOX, respectively. After 4-h's incubation, excess nanoparticles were washed away by PBS. Fresh complete DMEM medium was then added to the wells, and then the cells were incubated again in 5% CO_2 at 37 °C for 24 h. The cell viability was assessed by MTT assay.

K. Cellular internalization and intracellular trafficking of AFe-PEG/DOX

Hela cells were cultured in the complete DMEM in a culture disk at density of 2×10^5 cells at 37 °C with 5% CO_2 humidified atmosphere for 24 h. Then the culture medium was removed, and the cells were washed with PBS three times. Then, the cells were incubated with PBS containing AFe-PEG/DOX nanoparticles (10 μg/mL), DAPI and LysoTracker Green DND-26. After being incubated for different time (2, 4, 8, and 12 h), the cells were observed with a confocal laser scanning microscopy (CLSM) to record the fluorescence intensity at the specific wavelength excited by different laser, *i.e.*, the blue fluorescence of DAPI (400 nm at λ_{ex}=350 nm), green fluorescence of LysoTracker Green (511 nm at λ_{ex}=504 nm) and red fluorescence of DOX (591 nm at λ_{ex}=477 nm).

L. Magnetically targeted delivery of AFe-PEG/DOX

Hela cells were cultured in the complete DMEM in a culture disk at density of 2×10^5 cells at 37 °C with 5% CO_2 humidified atmosphere for 24 h. Then the culture medium was removed and washed with PBS three times. After that, the cells were incubated with PBS containing AFe-PEG/DOX nanoparticles (50 μg/mL) in the presence and absence of an external magnet for 2 h. Subsequently, the cells were rinsed with PBS buffer, and observed by CLSM. The intensity of red fluorescence of DOX at 591 nm excited by 477-nm laser was recorded.

III. RESULTS AND DISCUSSION

A. Preparation and characterization of cubic amorphous iron oxide (AFe) nanoparticles

Amorphous iron oxides are active enough to release Fe ions in mild acidic condition so as to induce localized Fenton reaction in the presence of H_2O_2 [28]. It can be prepared by the thermal decomposition of Prussian blue (PB) [27]. As illustrated in FIG. 1, uniform cubic PB nanoparticles with an edge length of about 170 nm were firstly prepared according to the previous report [26], as shown in FIG. 2(a) and FIG. S4(a) of supplementary materials. PB is a mixed-valence iron(III) hexacyanoferrate (II) compound of $Fe_4[Fe(CN)_6]_3$ with a face-centered-cubic (fcc) crystal structure [29]. During the calcination process in our work, the iron components of PB can be *in situ* oxidized. Only the organic components will be removed. Therefore, after cubic PB nanoparticles were calcinated at 400 °C in air for 4 h, the final AFe nanoparticles can keep the cubic morphology of PB nanoparticles except that they seem

DOI:10.1063/1674-0068/cjcp1906123 ©2020 Chinese Physical Society

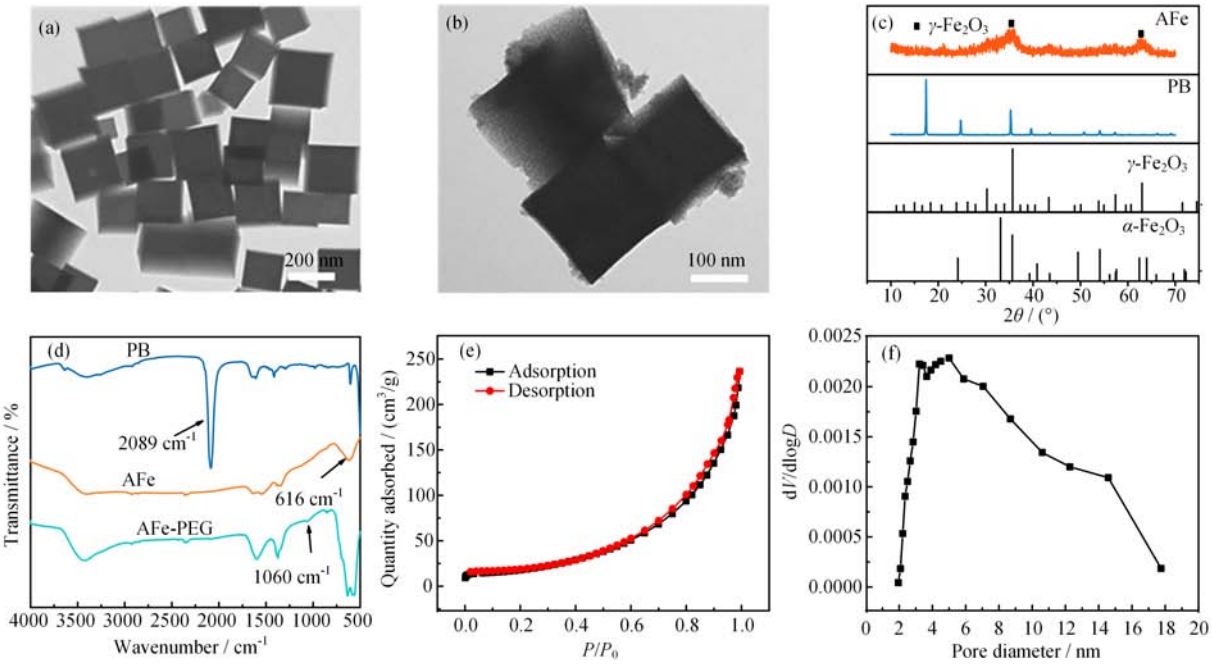

FIG. 2 TEM images of (a) PB and (b) AFe. (c) XRD and (d) FTIR spectra of PB and AFe nanoparticles. (e) N_2 adsorption-desorption isotherms and (f) BJH pore size distribution of AFe nanoparticles.

to have a porous structure (see FIG. 2 (b)) and the size distribution becomes a little wider (see FIG. S4(b) in supplementary materials), which accord with the results in another research [26]. However, the XRD and FTIR spectra of the nanoparticles before and after the calcination treatment, as shown in FIG. 2 (c) and (d) respectively, are totally different. The XRD pattern of the calcinated nanoparticles shows only two broad and weak diffraction peaks at 2θ=35° and 63°, which correspond to the main diffraction peaks of γ-Fe_2O_3 according to JCPDS card No.25-1402. Compared with the XRD pattern of PB, it indicates that PB has been almost converted into an amorphous iron oxide nanoparticles (AFe). Correspondingly, the characteristic absorption of -CN at 2089 cm^{-1} on the FTIR spectrum of PB disappears after the calcination treatment, while the absorption peak of Fe−O at 616 cm^{-1} appears, further proving the formation of AFe nanoparticles. The N_2 adsorption-desorption isotherms of AFe in FIG. 2(e) show a type IV curve with a type H3 hysteresis loop according to Brunauer-Deming-Deming-Teller (BDDT) classifications [30, 31], implying the presence of mesopores. The average pore diameter is 6.3 nm according to the Barrett-Joyner-Halenda (BJH) method, as shown in FIG. 2(f). The Brunauer-Emmett-Teller (BET) surface area is 68.7 m^2/g.

B. The PEG-modification and DOX loading of AFe nanoparticles

In order to improve the biocompatibility of the AFe nanoparticles as the drug carrier, PEG has been modified on the surface of AFe nanoparticles, as illustrated in FIG. 1. The new absorption peak appearing at 1060 cm^{-1} (C−O) on FTIR spectrum of AFe-PEG (FIG. 2(d)) confirms that the AFe nanoparticles are successfully modified with PEG-DA. The PEG-density of AFe-PEG nanoparticle is estimated to be 26.6 mg/m^2 according to the thermo-gravimetric analysis (TGA) result of AFe-PEG nanoparticles (FIG. S5 in supplementary materials). When AFe-PEG nanoparticles are dispersed into PBS (pH=7.4) containing DOX, the drug molecules can be loaded on the AFe-PEG nanoparticles through the coordinative bonding between the Fe ion and chemical groups (*e.g.*, amino and carbonyl) of DOX. The FTIR spectrum of AFe-PEG/DOX shows the characteristic adsorption of C=O groups on DOX at 1730 cm^{-1}, indicating the successful drug loading (FIG. 3(a)). The loading capacity of DOX (Q_{DOX}) is calculated to be 948 mg/g according to the UV-Vis spectroscopy method (FIG. 3(b) and Eq.(1)) which is much higher than some carriers reported in Ref.[32–34]. It may be related to the mesoporous structure with high specific area and pore volume of AFe matrix.

C. The release of DOX and Fe(III) ions from AFe-PEG/DOX nanoparticles

A perfect carrier should release its cargo at once when it is transferred from neutral to mildly acidic tumor microenvironment. The release behaviors of DOX from AFe-PEG/DOX in buffer solutions with different pH values are shown in FIG. 3(c), which reveals an obvious

DOI:10.1063/1674-0068/cjcp1906123 ©2020 Chinese Physical Society

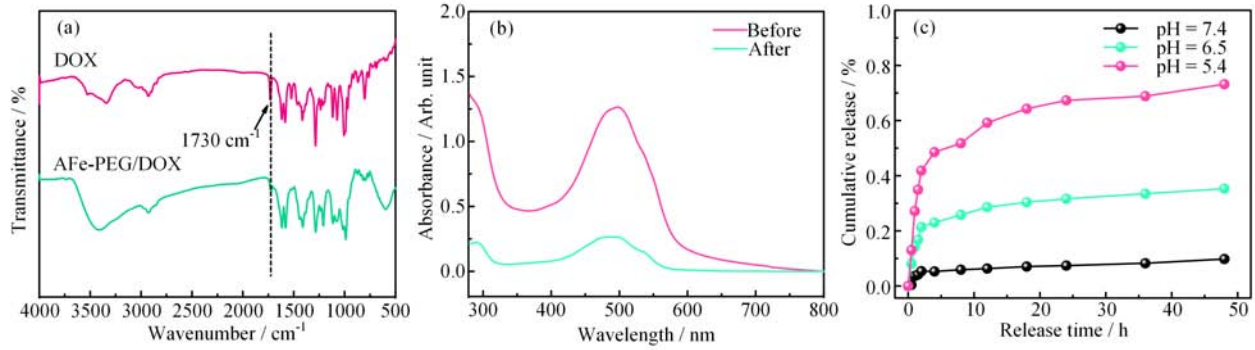

FIG. 3 (a) FTIR spectra of DOX and AFe-PEG/DOX nanoparticles. (b) UV-Vis spectra of the PBS (pH=7.4) solution of DOX (2 mg/mL) before and after the addition of AFe nanoparticles. (c) Release profiles of DOX from AFe-PEG/DOX under different pH values.

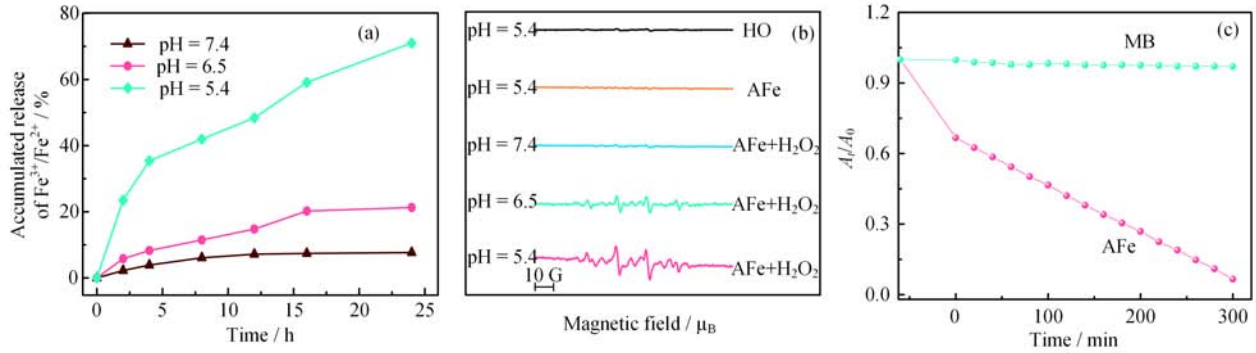

FIG. 4 (a) The real-time release percentage of Fe ion in PBS (at different pH) that contains AFe-PEG nanoparticles. (b) ESR spectra of different reaction systems with 5,5-dimethyl-1-pyrroline-N-oxide (DMPO) as the spin trap. (c) The real-time absorption of MB in acetate buffer solution (pH=5.4) containing H_2O_2 in the absence and presence of AFe-PEG nanoparticles.

pH-responsive release profile. The cumulative release percentage of DOX (q) increases with the decrease of pH of the buffer solution. It exceeds 70% in an acetate buffer (pH 5.4) after 48 h, but is less than 10% in PBS (pH 7.4). This should be attributed to the dissociation of metal-ligand coordination bonding at a low pH which favors the protonation of N and O atoms. However, when pH is 5.4, there are also some metal-ligand coordinations due to that the amino groups of DOX are not completely protonation, thus resulting in the final DOX release less than 100%.

At the same time, the Fe ion will be also released from AFe-PEG in the acid microenvironment. The release behaviors of AFe-PEG in buffer solutions with different pH are shown in FIG. 4 (a). The content of Fe element was determined by ICP-OES. The accumulated release of Fe ion after 24 h can reach 71% in an acetic buffer (pH=5.4), and 21% in PBS (pH=6.5), but only 8% in PBS (pH=7.4). The result means AFe-PEG nanoparticles can be expected to act as an effective Fenton reagent for the generation of hydroxyl radicals (·OH) in an acidic condition. Therefore, the ESR technique and the degradation of methylene blue (MB) are applied to confirm whether the Fenton-reaction of AFe-PEG and H_2O_2 can occur under acid conditions. As shown in FIG. 4(b), the ESR signals only occur at the condition of pH lower than 7. FIG. 4(c) shows clearly that the absorption intensity of MB in acetate buffer (pH=5.4) containing AFe-PEG and H_2O_2 drops rapidly as the time goes on. All the results prove that AFe-PEG nanoparticles can act as an effective Fenton agent in an acidic environment.

D. *In vitro* combined chemodynamic therapy and chemotherapy

According to the previous analysis, AFe-PEG/DOX nanoparticles can efficiently release Fe^{3+}/Fe^{2+} and DOX in an environment of low pH. Thus, the *in vitro* therapeutic efficiency of AFe-PEG/DOX nanocapsule was further investigated in detail (FIG. 5(a)). The MTT assay [35] was performed to measure the cell viabilities quantitatively after Hela cells were incubated with PBS, PBS containing free DOX and AFe-PEG/DOX, as shown in FIG. 5(b) and FIG. S6 (supplementary materials). Obviously, the cell viability decreases with the increase of the particle concentration. In contrast, the cell killing effect of single CDT (AFe-

DOI:10.1063/1674-0068/cjcp1906123 ©2020 Chinese Physical Society

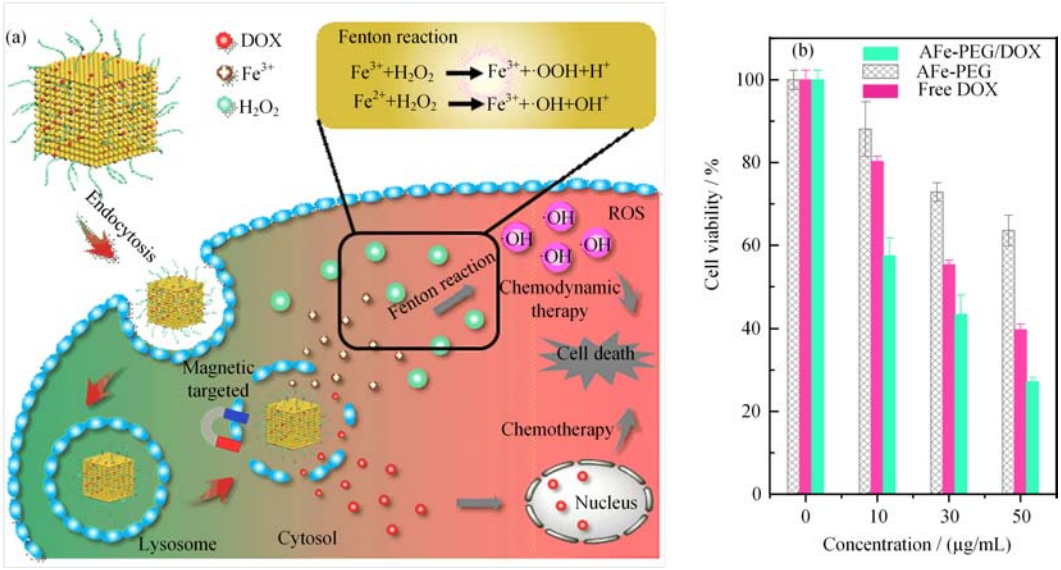

FIG. 5 (a) Illustration of the dual-mode chemo/chemodynamic therapy mechanism of AFe-PEG/DOX nanoparticles. (b) Cell viabilities of Hela cells after various therapeutic treatments.

PEG group) or CTT (DOX group) treatment is much lower than that of dual CTT/CDT (AFe-PEG/DOX group) treatment, suggesting that the AFe-PEG/DOX nanoparticles possess a combination therapeutic effect on cancer cells.

Furthermore, the cellular internalization and intracellular trafficking of AFe-PEG/DOX nanoparticles are observed with CLSM, as shown in FIG. 6(a) and FIG. S7 in supplementary materials. Within the first 4-h's incubation, the red fluorescence of AFe-PEG/DOX nanoparticles only occurred at the area of cytoplasm since it overlapped well with the green channel of LysoTracker green (labelled endosome/lysosome), indicating AFe-PEG/DOX nanoparticles located in lysosome. However, it can be observed gradually from cytoplasm to cell nuclei with the extension of the incubation time, demonstrating the release of DOX. The relative fluorescence intensities of DOX in nuclei and the colocalization ratios of red channel (DOX) to green channel (LysoTracker green) fluorescence calculated from FIG. 6(a) are displayed in FIG. 6 (b) and (c). It can be seen from FIG. 6(b) that the intensity of red fluorescence of DOX in nuclei increases almost 12-fold when the incubation time increases from 2 h to 12 h. Meanwhile, the colocalization ratio of red channel to green channel shows a monotonous drop from 79% to 37% during the same incubation time scale, suggesting the loaded DOX on the internalized AFe-PEG/DOX nanoparticles releases gradually in the acidic tumor microenvironment.

E. *In vitro* magnetically targeted drug delivery

The magnetism of the prepared AFe-PEG nanoparticle is evaluated by vibrating sample magnetometer (VSM), as shown in FIG. 7(a). The saturation magnetization (M_s) of AFe nanoparticle is 58.6 emu/g, which is enough for AFe-PEG nanoparticle to be separated in PBS by a magnet. The delivery efficiency of AFe-PEG/DOX nanoparticles in Hela cells for 2-h' incubation under an external magnetic field was investigated, as shown in FIG. 7(b). It can be seen that the red fluorescence of DOX in the cells increases remarkably, compared with that in the cells incubated without an external magnetic field. The quantitative fluorescence intensity of DOX calculated from FIG. 7(b) is listed in FIG. 7 (c), which clearly demonstrates that the AFe-PEG/DOX nanoparticles can be of potential use for magnetically targeted drug delivery.

IV. CONCLUSION

In summary, a versatile polyethylene glycol (PEG) modified amorphous iron oxides (AFe) nanoparticle (AFe-PEG) was prepared as the carrier of doxorubicin (DOX). The AFe-PEG nanoparticles possess extraordinarily high DOX loading capacity of 948 mg/g, due to the mesoporous structure with high specific area and strong coordinative bonding between Fe ions and chemical groups (*e.g.*, amino and carbonyl) of DOX. In an acidic microenvironment, the AFe-PEG/DOX naoparticles will release not only DOX efficiently, but also Fe ions which induce a Fenton reaction. *In vitro* experimental results suggested that the AFe-PEG/DOX nanoparticles can achieve a combination of chemotherapeutic (CTT) and chemodynamic therapeutic (CDT) effect on Hela cells, resulting in an enhanced killing effect on cancer cells. In addition, AFe-PEG/DOX nanoparticles exhibit an improved cellular internaliza-

DOI:10.1063/1674-0068/cjcp1906123 ©2020 Chinese Physical Society

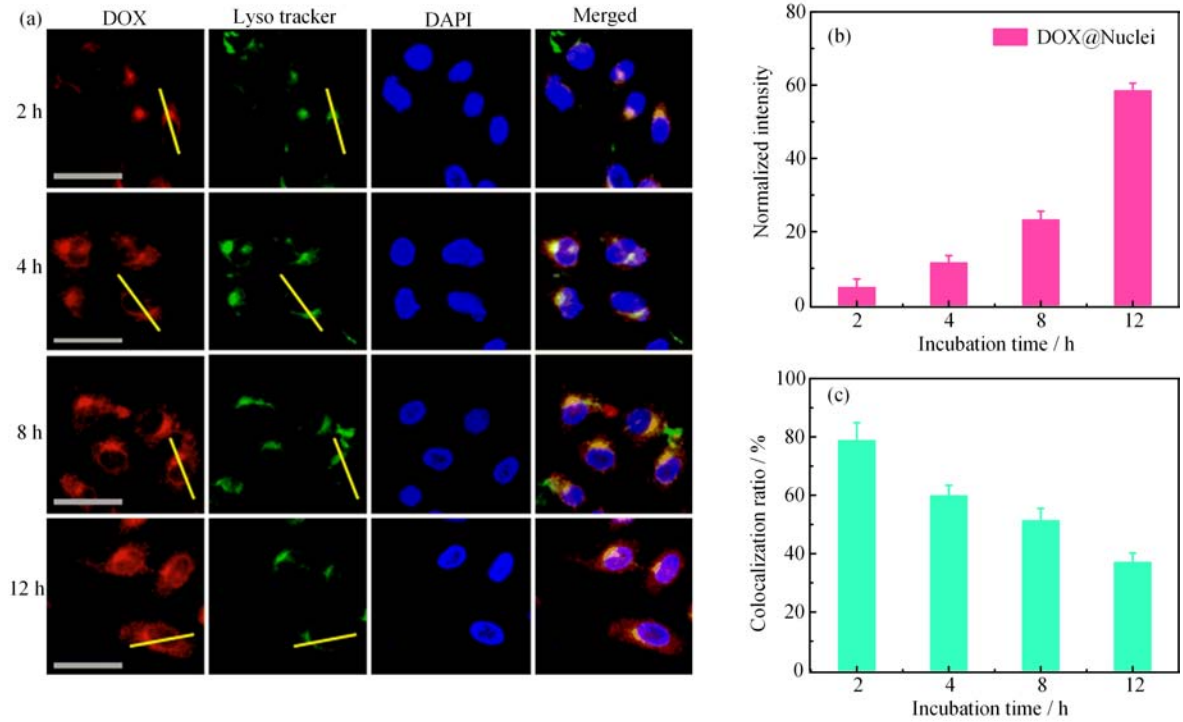

FIG. 6 (a) Representative CLSM images of Hela cells incubated in PBS for 2, 4, 8, and 12 h after the cells had been incubated with AFe-PEG/DOX nanoparticles for 2 h. The cells were co-stained with LysoTracker green (green channel) and DAPI (blue channel). Scale bar is 50 μm. (b) Relative fluorescence intensities of DOX in nuclei and (c) the colocalization ratios of red channel (DOX) and green channel (LysoTracker green) fluorescence deduced from (a).

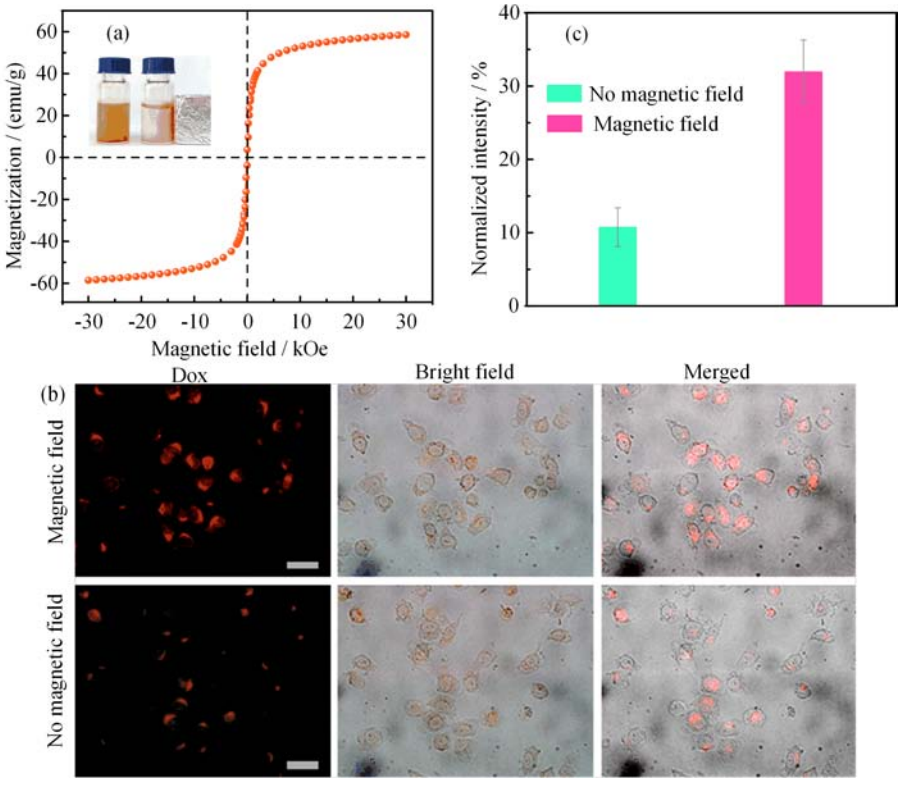

FIG. 7 (a) VSM of AFe-PEG nanoparticles. Inset: digital photos of PBS containing AFe-PEG nanoparticles with and without a magnetic field. (b) Representative CLSM images of Hela cells after 2-h's incubation in PBS containing AFe-PEG/DOX in the presence and absence of an external magnetic field. Scale bar is 50 μm. (c) Normalized fluorescence intensities (red channel) of Hela cells calculated from (b).

DOI:10.1063/1674-0068/cjcp1906123 ©2020 Chinese Physical Society

tion performance, showing a potential use for magnetically targeted drug delivery. Therefore, this work develops a new and promising magnetically targeted delivery and dual CTT/CDT therapeutic nano-medicine platform based on amorphous iron oxide.

Supplementary materials: Synthesis and characterization of compounds employed in this work, working curve of DOX, characterization of nanoparticles, thermo-gravimetric analysis (TGA) of nanoparticles, the Fluorescence images of Hela cells, the cellular internalization and intracellular trafficking of DOX are shown.

V. ACKNOWLEDGMENTS

We thank Ms. Y. X. Bai in the Hefei National Laboratory for Physical Sciences at the Microscale of University of Science and Technology of China for their kind help in characterization of thermo-gravimetric analysis (TGA). This work was supported by the National Natural Science Foundation of China (No.51473152 and No.51573174), Scientific Research Foundation for Young Talents from Fujian Provincial Department of Education (No.JT180494), and Scientific Research Platform Construction Project from Fujian Provincial Department of Science and Technology (No.2018H2002).

[1] T. Iwamoto, Biol. Pharm. Bull. **36**, 715 (2013).
[2] D. Peer, J. M. Karp, S. Hong, O. C. Farokhzad, R. Margalit, and R. Langer, Nat. Nanotechnol. **2**, 751 (2007).
[3] R. Mo, T. Jiang, R. DiSanto, W. Tai, and Z. Gu, Nat. Commun. **5**, 3364 (2014).
[4] T. M. Sun, Y. S. Zhang, B. Pang, D. C. Hyun, M. X. Yang, and Y. N. Xia, Angew. Chem. Int. Ed. **53**, 12320 (2014).
[5] X. W. Zeng, G. Liu, W. Tao, Y. Ma, X. D. Zhang, F. He, J. M. Pan, L. Mei, and G. Q. Pan, Adv. Funct. Mater. **27**, 1605985 (2017).
[6] L. Huang, L. Ao, D. H. Hu, W. Wang, Z. H. Sheng, and W. Su, Chem. Mater. **28**, 5896 (2016).
[7] X. J. Cai, X. Q. Jia, W. Gao, K. Zhang, M. Ma, S. G. Wang, Y. Y. Zheng, J. L. Shi, and H. R. Chen, Adv. Funct. Mater. **25**, 2520 (2015).
[8] X. J. Cai, W. Gao, M. Ma, M. Y. Wu, L. L. Zhang, Y. Y. Zheng, H. R. Chen, and J. L. Shi, Adv. Mater. **27**, 6382 (2015).
[9] S. Mura, J. Nicolas, and P. Couvreur, Nat. Mater. **12**, 991 (2013).
[10] H. J. Xiang, H. Lin, L. D. Yu, and Y. Chen, ACS Nano **13**, 2223 (2019).
[11] W. X. Sun, H. T. Jiang, X. Wu, Z. Y. Xu, C. Yao, J. Wang, M. Qin, Q. Jiang, W. Wang, D. Q. Shi, and Y. Cao, Nano Res. **12**, 115 (2018).
[12] Y. X. Guo, Y. Zhang, J. Y. Ma, Q. Li, Y. Li, X. Y. Zhou, D. Zhao, H. Song, Q. Chen, and X. Zhu, J. Control. Release **272**, 145 (2018).
[13] P. Mi, D. Kokuryo, H. Cabral, H. L. Wu, Y. Terada, T. Saga, I. Aoki, N. Nishiyama, and K. Kataoka, Nat. Nanotechnol. **11**, 724 (2016).
[14] S. Lei, J. X. Chen, K. Zeng, M. Z. Wang, and X. W. Ge, Nano Res. **12**, 1071 (2019).
[15] C. M. Yu, L. H. Qian, J. Y. Ge, J. Q. Fu, P. Y. Yuan, S. C. L. Yao, and S. Q. Yao, Angew. Chem. Int. Ed. **55**, 9272 (2016).
[16] Y. Q. Zhang, J. Q. Wang, J. C. Yu, D. Wen, A. R. Kahkoska, Y. Lu, X. D. Zhang, J. B. Buse, and Z. Gu, Small **14**, e1704181 (2018).
[17] M. Ahlen, G. K. Tummala, and A. Mihranyan, Int. J. Pharm. **536**, 73 (2018).
[18] H. R. Wang, W. W. Zhu, J. J. Liu, Z. L. Dong, and Z. Liu, ACS Appl. Mater. Interfaces **10**, 14475 (2018).
[19] X. D. Xue, Y. Huang, R. Bo, B. Jia, H. Wu, Y. Yuan, Z. L. Wang, Z. Ma, D. Jing, X. B. Xu, W. M. Yu, T. Y. Lin, and Y. P. Li, Nat. Commun. **9**, 3653 (2018).
[20] X. Zhang, X. H. Xu, Y. C. Li, C. Hu, Z. J. Zhang, and Z. W. Gu, Adv. Mater. **30**, e1707240 (2018).
[21] J. Z. Du, X. J. Du, C. Q. Mao, and J. Wang, J. Am. Chem. Soc. **133**, 17560 (2011).
[22] Q. Chen, C. Wang, X. D. Zhang, G. J. Chen, Q. Y. Hu, H. J. Li, J. Q. Wang, D. Wen, Y. Q. Zhang, Y. F. Lu, G. Yang, C. Jiang, J. Wang, G. Dotti, and Z. Gu, Nat. Nanotechnol. **14**, 89 (2019).
[23] J. Nam, S. Son, L. J. Ochyl, R. Kuai, A. Schwendeman, and J. J. Moon, Nat. Commun. **9**, 1074 (2018).
[24] Y. L. Dai, Z. Yang, S. Y. Cheng, Z. Y. Wang, R. L. Zhang, G. Z. Zhu, Z. T. Wang, B. C. Yung, R. Tian, O. Jacobson, C. Xu, Q. Q. Ni, J. B. Song, X. L. Sun, G. Niu, and X. Y. Chen, Adv. Mater. **30**, 1704877 (2018).
[25] J. X. Chen, S. Lei, K. Zeng, M. Z. Wang, A. Asif, and X. W. Ge, Nano Res. **10**, 2351 (2017).
[26] M. Hu, S. Furukawa, R. Ohtani, H. Sukegawa, Y. Nemoto, J. Reboul, S. Kitagawa, and Y. Yamauchi, Angew. Chem. Int. Ed. **51**, 984 (2012).
[27] M. Hu, A. A. Belik, M. Imura, K. Mibu, Y. Tsujimoto, and Y. Yamauchi, Chem. Mater. **24**, 2698 (2012).
[28] J. L. Shi, Nanomedicine **11**, 1189 (2016)
[29] L. Zhang, H. B. Wu, S. Madhavi, H. H. Hng, and X. W. Lou, J. Am. Chem. Soc. **134**, 17388 (2012).
[30] K. S. W. Sing, Pure Appl. Chem. **57**, 603 (1985).
[31] S. Brunauer, L. S. Deming, W. E. Deming, and E. Teller, J. Am. Chem. Soc. **62**, 1723 (1940).
[32] Y. F. Zhu, J. L. Shi, W. H. Shen, X. P. Dong, J. W. Feng, M. L. Ruan, and Y. S. Li, Angew. Chem. Int. Ed. **44**, 5083 (2005).
[33] W. R. Zhao, H. R. Chen, Y. S. Li, L. Li, M. D. Lang, and J. L. Shi, Adv. Funct. Mater. **18**, 2780 (2008).
[34] Y. Chen, H. R. Chen, D. P. Zeng, Y. B. Tian, F. Chen, J. W. Feng, and J. L. Shi, ACS Nano **4**, 6001 (2010).
[35] F. X. Lin, K. Zeng, W. X. Yang, M. Z. Wang, J. L. Rong, J. Xie, Y. Zhao, and X. W. Ge, Chin. J. Chem. Phys. **30**, 231 (2017).

DOI:10.1063/1674-0068/cjcp1906123 ©2020 Chinese Physical Society